Synthesis of open-cell metal foams by templated directed vapor deposition

Douglas T. Queheillalt, Derek D. Hass, David J. Sypeck, and Haydn N.G. Wadley
Department of Materials Science and Engineering, School of Engineering and Applied Science,
University of Virginia, Charlottesville, Virginia 22904

Low-density, open-cell nickel base superalloy foams have been synthesized by a high-rate, electron beam-directed vapor deposition process and their mechanical properties evaluated. The deposition process uses an open-cell polymer foam template upon which is deposited a metal alloy coating. The electron beam evaporated flux was entrained in a rarefied transonic gas jet and propagated along the flow stream lines through the polymer structure. After vapor deposition, the polymer template was removed by low-temperature thermal decomposition. The resultant ultralightweight metal foams consisted of a three-dimensional open cell, reticulated structure possessing hollow triangular ligaments with relative densities of <3%. Their mechanical integrity was increased by either pressureless or transient liquid phase sintering. The mechanical properties of these ultralightweight metal foams were comparable to theoretical predictions for open-cell, reticulated foams.

I. INTRODUCTION

Ultralightweight cellular solids can be manufactured from numerous metals and metal alloys by a wide variety of methods.[1] The properties of these materials depend upon the properties of the metal, the relative density of the foam, and the distribution of material within the foam (e.g., open or closed cell, cell size, etc.)[2-4] Closed-cell metal foams possess high modulus and strength characteristics, high impact energy absorbing characteristics,[5,6] very low thermal conductivities,[7] and excellent acoustic damping characteristics,[8,9] when compared with the metal from which they are made. Open-cell foams are not as stiff or as strong, but they posses characteristics which can be exploited in multifunctional load supporting and heat dissipation applications because of the ability to flow fluids readily through the heated structure.[10,11] They also have a high surface area to volume ratio and can be used as high-temperature supports for catalysts and electrodes in electrochemical cells.

Numerous solid- and liquid-state processes have been developed for the manufacture of closed-cell metal foams and porous solids. These include melt gas injection, gas releasing particle decomposition in melts and semisolids, gas metal eutectic solidification, and entrapped gas expansion.[1] These methods result in foams with cell sizes ranging from 100 μm to 5 cm and relative densities from 0.05 to 1.0. The synthesis of open-cell metal foams can be accomplished by investment casting using an open-cell mold,[12] electrolytic deposition,[13-19] and chemical[20] or physical[22-24] vapor deposition

on polymer templates. The as-deposited structures are subjected to a low-temperature thermal treatment during which the parent polymer template is thermally decomposed. This is usually followed by a high-temperature sintering treatment to densify the ligaments. These methods result in foams with cell sizes ranging from 100 μm to 5 mm and relative densities from 0.01 to 0.15.

The electrolytic deposition process involves the dissolution of one electrode (an anode) and the deposition of this metal on a second electrode (the polymer template cathode). Because polymer-based foams are nonconductive, they must be made electrically conductive by either sputtering or ionic deposition. The metal foam is then created by the subsequent electrolytic deposition of elemental Ni or Cu. Metal foams produced by this method are currently manufactured under the trade names Celmet (Sumitomo Electric, Osaka, Japan) and Metapore (Sociètè Sorapec, Fontenay Sous Bois, France) for use in Ni–Cd and Ni–metal hydride batteries and catalytic devices. A major limitation of electroless deposition processes is that deposition is limited to a few metallic elements (alloys are difficult). In addition, deposition rates are low (approximately 0.2–2.0 μm/min), and nonuniform deposition may occur due to uneven field distributions over irregular shaped objects. The resultant foams often exhibit poor physical and mechanical properties because of their pure metal composition.

Chemical vapor deposition (CVD) of a metal carbonyl gas has also been used to manufacture metal foams.[20-22] Pure (>99 wt% Ni) metal foams manufactured by

thermal decomposition of Ni(CO$_4$) gas are produced by Inco Limited (Toronto, Ontario, Canada) under the trade name Incofoam. It is increasingly used for the nickel electrode of rechargeable batteries. Refractory metal foams (i.e., Zr, Nb, Hf, Ta, W, and Re) produced by chemical vapor infiltration (CVI) are also manufactured by Ultramet Advanced Materials (Pacoima, CA) and Recemat International (The Netherlands) under the trade names Ultrametal and Recemat. Potential applications include thermal insulation, lightweight nozzle flaps for advanced turbine engines, aerobraking structures, aircraft wing and fuselage structures, molten metal, and catalytic filtration devices. Advantages of the CVD and CVI processes include high throwing power resulting in high deposition rates, non-line-of-sight deposition, relatively inexpensive capital equipment costs (because it is a low-vacuum process) and the ability to deposit both elemental metals and some alloys. However, vapor decomposition of the least expensive chemical precursors occurs at high temperatures where the thermal stability of the polymer template must be taken into consideration. The need to use toxic, low decomposition temperature chemical precursors results in a costly process that is difficult to implement in an environmentally satisfactory manner.

Physical vapor deposition (PVD) techniques including metal spray deposition, thermal evaporation, reactive sputtering, and arc-vapor deposition have also been used to manufacture metal foams.[22–24] The arc-vapor deposition process developed by Vapor Technologies, Inc. (Boulder, CO), and other conventional PVD processes investigated by Montedison (Milan, Italy) have been patented in recent years. However, PVD processes such as these offer a number of potential advantages including the ability to deposit most metal elements and many of their alloys and to even create foams with multilayered or functionally graded metal ligaments. However, because these processes operate in high vacuum (10^{-5}–10^{-9} torr), they coat only the surfaces that are in the line-of-sight of the vapor source. This is likely to result in uneven coating of the polymer template, depending on the cell size. In addition, low deposition rates (less than 2 μm/min), low materials utilization factors, and difficulties in maintaining stoichiometry for alloys whose constituents possess widely varying vapor pressures can impose constraints upon the use of conventional PVD techniques for the low-cost synthesis of metal foams.

Here, we explore the application of an electron beam-directed vapor deposition (EB-DVD) approach for synthesizing open cell metal alloy foams. In the EB-DVD approach, electron beam-evaporated vapor is entrained in a rarefied transonic gas jet and propagated through a polymer foam template. We show that low-density metal foams can be created in this manner and report on the mechanical properties of foams made from a high-temperature, corrosion resistant nickel-based superalloy.

II. DEPOSITION METHODOLOGY

Electron beam evaporation is a widely used method for the high-rate production of atomic and molecular vapor.[25] Normally, vapor is ballistically transported to a substrate under high-vacuum conditions where it condenses on surfaces that are in the line-of-sight of the flux source. However, by intersecting the vapor plume with a rarefied trans- or supersonic inert gas jet, it is possible to entrain the evaporated flux in a nonreacting gas flow and transport it to a substrate under low-vacuum (0.1–10 torr) conditions.[26,27] Deposition of the atomistic flux then occurs by gas phase scattering from the stream lines of the flow.[28] A schematic illustration of such an electron beam-directed vapor deposition (EB-DVD) process is shown in Fig. 1. The system used for deposition consisted of a 60 kV/10 kW axial electron beam gun (modified to function in a low vacuum environment) and a He carrier gas jet. A more complete description of the EB-DVD system and its available processing range can be found elsewhere.[28,29]

When the gas jet intersects an object, the stream lines pass around the object. Scattering of the condensable flux from this flow then enables non-line-of-sight deposition.
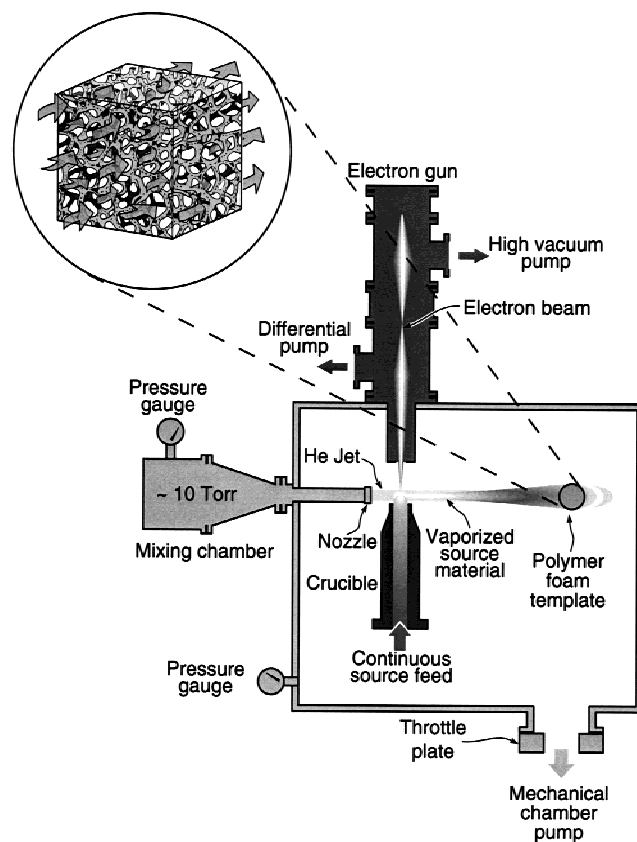

FIG. 1. Schematic diagram of the EB-DVD processing chamber showing the introduction of a carrier gas flow into the chamber through a nozzle which transports the evaporated source material through the polymer template.

The degree to which blind surfaces can be coated is a complicated function of the objects shape, the flow field near it, the composition of the flow, and the collision cross section of the material to be deposited. As a result, there exists an optimal set of process conditions that are best suited for each objects coating. These are controlled by the electron beam power and scan pattern on the metal source, the gas inlet nozzle flow pressure, the operating chamber pressure, and the nozzle geometry. These can all be significantly varied facilitating wide processing condition variations.

For the deposition experiments reported here, cylindrical samples were used (25.4 mm in length and 12.7 mm in diameter) as the deposition template. They consisted of open-cell, reticulated polyurethane foams with a pore size of approximately 0.85 mm (30 pores/in. nominal). The polymer foam was positioned 7.0 cm from the nozzle and 5.0 cm from the vapor source. The polymer foam templates were rotated about its cylindrical axis at approximately 1 revolution/min and also translated axially through the vapor flux region to promote uniform deposition and complete infiltration. Several trial deposition experiments were conducted using different combinations of upstream and process chamber pressures and gas flow rates. At low process pressures (0.30 torr), flux scattering from the stream lines resulted in thick coatings at the exterior of the sample. Very low process pressures enhance line-of-site coating and incomplete coverage of ligaments. Intermediate process pressures of 0.07 torr resulted in best ligament coating uniformity. The final operating conditions selected for the deposition used an electron beam power = 2100 W, He gas flow = 3.5 standard L/min, chamber pressure = 0.07 torr, and upstream nozzle pressure = 0.68 torr. During deposition, some heating of the substrate occurred. The process conditions ensured the temperature remained below approximately 100 °C to prevent slumping of the polymer template during deposition. Variation of the deposition time allowed the metal thickness to be varied.

An Inconel alloy 625 nickel-based superalloy of nominal composition Ni–21.3 Cr–8.8 Mo–3.9 Nb–0.13 Al–0.19 Ti wt% was used for deposition. Conventional ingot processed Inconel alloy 625 is a non-age-hardenable, solid solution alloy with a face centered cubic (γ-phase) crystal structure. It is microstructurally stable up to 650 °C. The high alloying element concentrations make the alloy well suitable for high-temperature applications where corrosion and especially pitting resistance are required. Nominal properties for the fully dense polycrystalline alloy are the following: yield strength, σ_{ys} = 414 MPa; Young's modulus, E = 208 GPa; shear modulus, G = 81 GPa; density, ρ = 8.44 g/cm^3.[30]

After deposition, the polymer template was removed by a thermal decomposition step. Typically, metal foam manufacturers remove the polymer templates by heating

in an atmosphere containing oxygen. The burnout conditions determine the amount of residual carbon which remains to potentially contaminate the metal foam. Various decomposition approaches have been explored. In one, the polymer was heated at approximately 1 °C/min or less to a temperature between 350 and 500 °C in air.[15,23] In another, metal-coated polymer templates were rapidly exposed (less than about 5 s) to a temperature of at least 600 °C (in air) to thermally decompose the polymer template. This latter process caused the gaseous oxidation products to form a large internal pressure and created burst holes in the metal layer.[33] Here, the polyurethane templates were removed by thermally decomposing the polymer in vacuum (approximately 10^{-5} torr) by heating at 1 °C/min to 250 °C and holding for 2 h. This resulted in complete removal of the polymer core with minimal carbon residue.

After thermal decomposition, the samples were either pressureless sintered or transient liquid-phase sintered. Pressureless sintering consisted of heating the samples at a rate of 10 °C/min up to 1150 °C, holding for 12 h followed by furnace cooling at approximately 25 °C/min in vacuum (approximately 10^{-5} torr). For transient liquid phase sintering, an alloy powder with a nominal composition of Ni–25.0 Cr–10.0 P–0.03 C wt% (Nicrobraz 51) was used. To apply this liquid phase sintering material, 40–100-μm-diameter braze powder was mixed with a binder and applied throughout the foam using an air powered fluidized bed. The samples were then heated at a rate of 10 °C/min up to 550 °C, holding for 1 h (to volatilize the binder), and then continued heating to 1120 °C, holding for 2 h followed by furnace cooling at approximately 25 °C/min. In all cases, the mass of liquid-phase sintering agent added was less than 5% of the mass of deposited metal foam.

The morphology of the EB-DVD foam structures was evaluated by scanning electron microscopy (SEM) and focused ion beam microscopy (FIB). X-ray diffraction (XRD) patterns and the lattice parameters (evaluated from {111} peaks) were obtained using Cu K$_\alpha$ radiation and a scan rate of 0.02 deg/min. The mechanical properties of the foams were determined using uniaxial compression tests at a strain rate of 0.024 min^{-1}. Because the initial loading of a metal foam may not accurately represent the true elastic modulus, each foam was loaded and unloaded at 2, 4, 6, 8, and 10% strain and the Young's modulus was calculated from the unloading curve.

III. RESULTS AND DISCUSSION

A. Coating morphology

The morphology of the directed vapor-deposited foam and the polymer template used for its synthesis is shown in Fig. 2. It can be seen in Fig. 2(a) that the reticulated

polymer foam template had cusp-shaped ligaments with triangular cross sections. The as-deposited metal foam therefore had hollow ligaments with cusp-shaped triangular interior voids, Fig. 2(b). The metal thickness was found to be similar on each of the three sides of the ligaments. However, some thickening at the apex was observed. This appears to be a manifestation of the higher flux view factor at these locations. Sectioning indicated that the coating thickness decreased slowly with depth into the foam. For the samples synthesized here, the coating thickness on interior ligaments was approximately 20% less than that on ligaments located on the samples exterior. Therefore, we expect interior located cells to be more compliant than cell located around the circumference of the samples.

B. Microstructural analysis

1. As-deposited condition

The morphology of the EB-DVD foams in the as-deposited condition is shown in Fig. 3. The as-deposited microstructure had a fractal surface created by the competitive growth of tapered columns, Fig. 3(a). The primary domed surface features were approximately 5 μm in diameter and in some cases exhibited intercolumnar cracking, Fig. 3(b). Some of the tapered columns extended from the substrate to the coating surface while others had nucleated in the coating and extended to the surface, Fig. 4. In general, the intercolumnar cracking was locally perpendicular to the deposition surface.
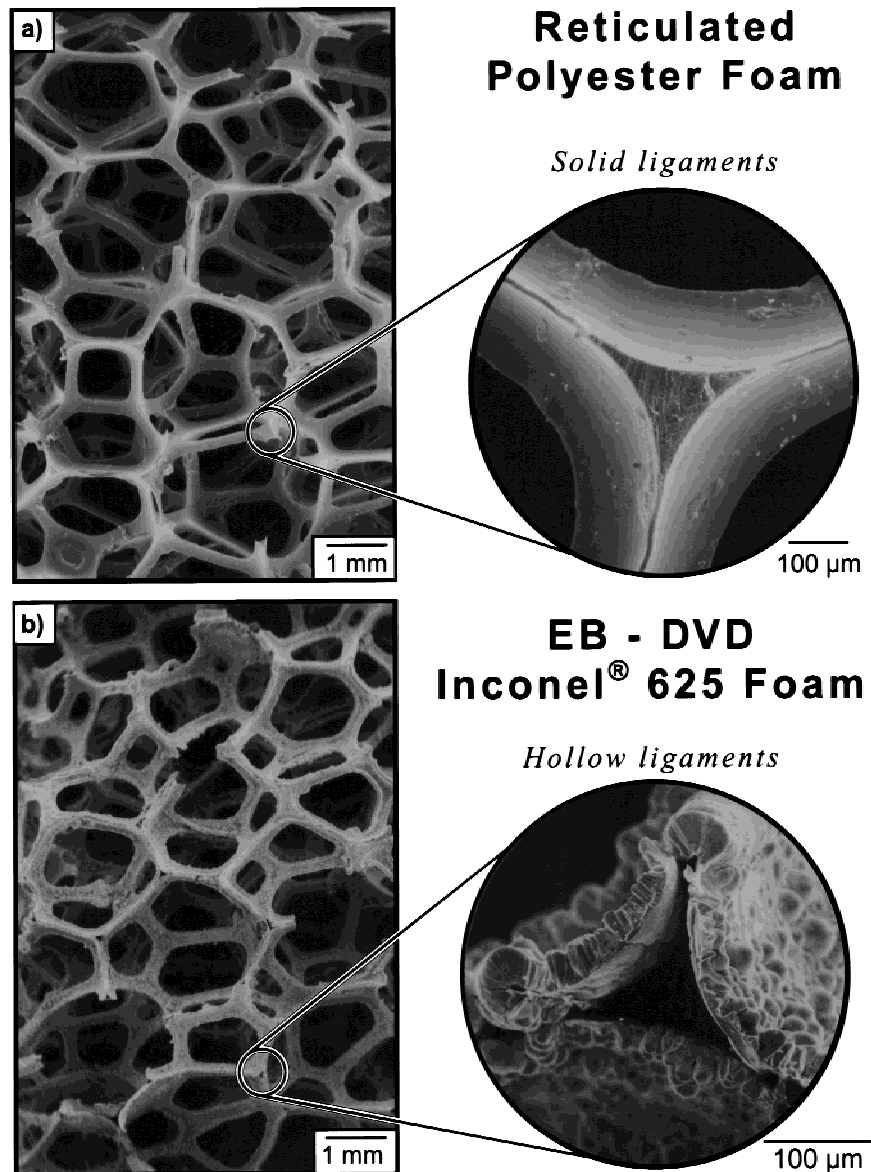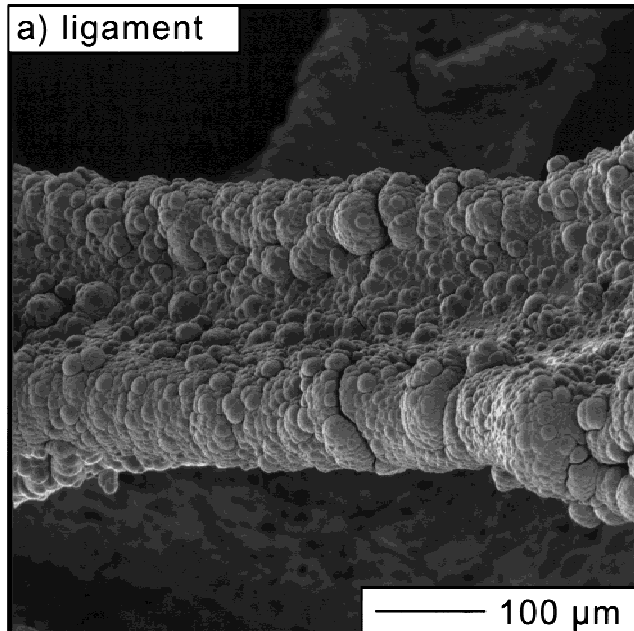

FIG. 2. Micrographs showing the structure of (a) the parent reticulated polymer foam with solid ligaments and (b) the EB-DVD metal foam possessing hollow ligaments after the thermal decomposition treatment.
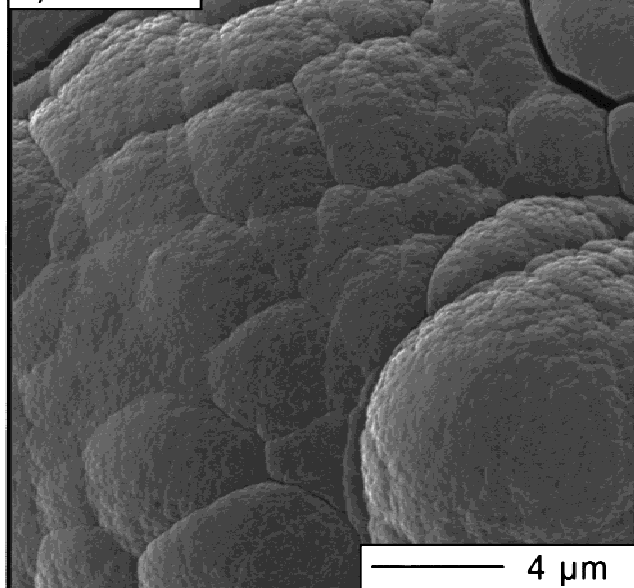
As deposited

a) ligament

100 µm

b) surface

4 µm

FIG. 3. Focused ion beam micrographs showing (a) the ligament structure and (b) the surface structure in the as-deposited condition.

as deposited

15 µm

FIG. 4. Focused ion beam micrograph showing the ligament cross section in the as-deposited condition.

The morphology of vapor-deposited coatings is controlled by four basic processes: shadowing (i.e. interaction between the roughness of the growing surface and the angular directions of the arriving coating atoms); surface diffusion; bulk diffusion; desorption of deposited atoms. Structure zone models (SMZs) for evaporated and sputter deposited metals can be used to characterize the structure of vapor-deposited films.[34–36] These empi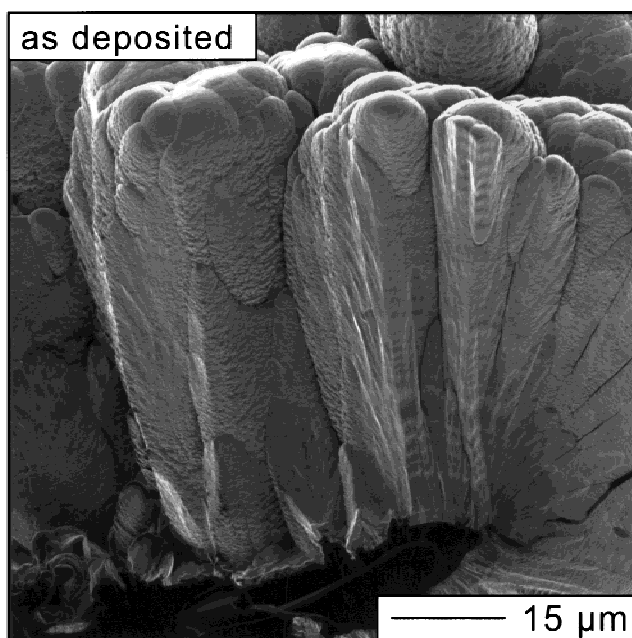rical models link characteristic structural forms (where the various growth mechanisms dominate) to zones of T/T_m (where T is the substrate temperature during deposition and T_m is the coating material's melting point) and inert gas pressure. Their contributions depend upon the homologous temperature of the film during growth, the deposition rate, the incidence angle distribution of the condensing flux, and characteristics of any energetic assisting ions.[37]

For the metal foams synthesized here, the deposition temperature was 0.2 T/T_m which is in the region labeled zone T (where, $0.1 < T/T_m < 0.3$); however, the structures exhibited characteristics more reminiscent of a zone 1 structure ($T/T_m < 0.1$). Zone 1 structures consist of tapered crystals with domed tops which are separated by voided boundaries.[34–36] The internal structure of these crystals are poorly defined, with a high dislocation density. The coatings are characterized by high hardness and low lateral strengths. This was observed by the fragility of the as-deposited foams. Zone 1 structures generally result when adatom diffusion is insufficient to overcome the effects of shadowing. Shadowing induces open boundaries because high points on the growing surface receive more coating flux than valleys do, particularly when a significant oblique component is present. The sometimes significant intercolumnar porosity (and resulting zone 1 structure) observed here appears to be a result of the very high effective angle of deposition and the high rate of deposition. The very oblique flux promotes shadowing while the high deposition rate leads to insufficient time for surface diffusion.[38]

2. Vacuum-sintered condition

Post deposition sintering was explored as a method to reduce some of the porosity. The morphology of the EB-DVD foams after pressureless sintering is shown in Fig. 5. The ligament structure, shown in Fig. 5(a), was more uniform than the as-deposited condition, but many pores with low curvatures remained. When the surface was examined at higher magnification, Fig. 5(b), the domed surfaces were seen to have formed a terraced
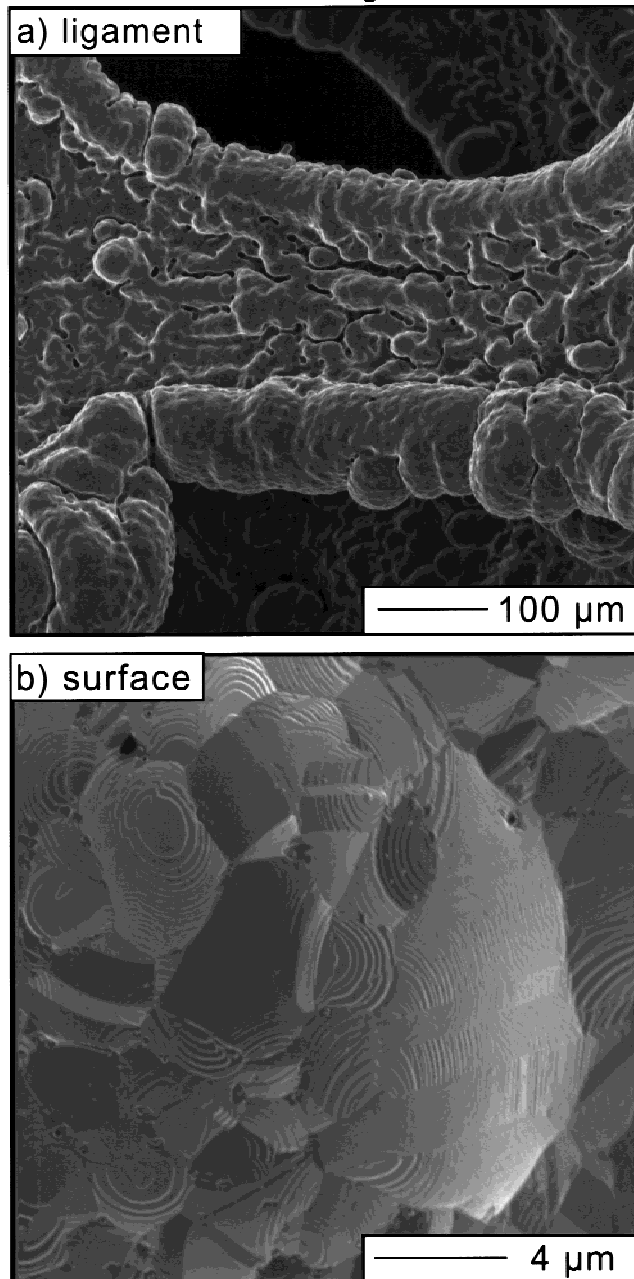
surface with a decreased surface energy.[39,40] Very little grain growth had occurred. The average grain size of the sintered structure was about the same as the as-deposited material and was less than 6 μm in diameter.

3. Transient liquid-phase sintered condition

The morphology of the EB-DVD foams after transient liquid phase sintering (TLPS) is shown in Fig. 6. A marked difference was observed in ligament and grain

FIG. 5. Focused ion beam micrographs showing (a) the ligament structure and (b) the surface structure after transient liquid phase sintering.
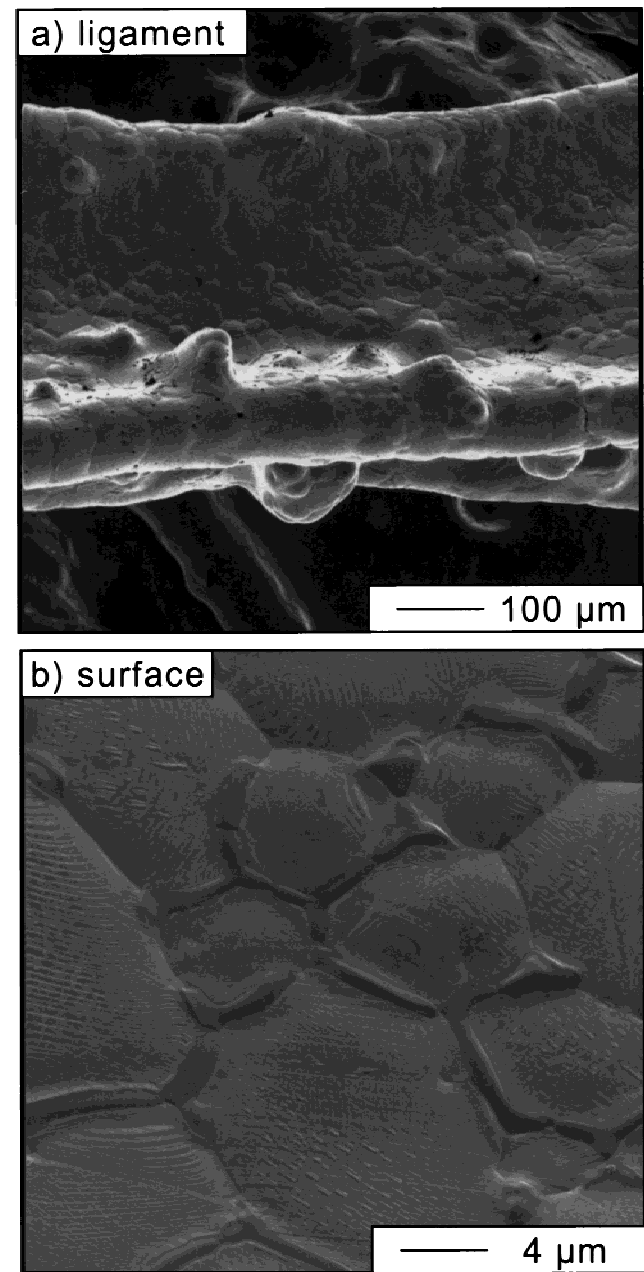

FIG. 6. Focused ion beam micrographs showing (a) the ligament structure and (b) the surface structure after transient liquid phase sintering.

structure when compared with the pressureless sintered samples. In the transient liquid phase process, a low melting temperature eutectic liquid forms as the melting point depressant (MPD) dissolves the base material and spreads through capillary action as the sample is heated to the bonding temperature.[41,42] The liquid films undergoes isothermal solidification as the MPD diffuses into the base metal at a rate dependent on the diffusion constants in the bulk. The fluid film aids densification and reduces porosity and defect concentrations (i.e., pinholes, cracks, fissures), Fig. 6(a). During this solution reprecipitation step microstructural coarsening occurs, and significant grain growth was observed, Fig. 6(b). This occurs because the solubility of a grain in its surrounding liquid varies inversely with the grains size; small grains have a higher solubility than coarse grains. The difference in solubility establishes a concentration gradient in the liquid, and material is transported from the small grains to the large grains by diffusion. The net result is a progressive growth of larger grains with an average grain diameter of less than 12 μm in diameter.

C. X-ray diffraction

X-ray diffraction patterns of Inconel alloy 625 for a random powder distribution, the initial bar used for evaporation, and the as-deposited EB-DVD coating were analyzed. All of the XRD patterns display characteristics of a high Ni face centered cubic alloy. The lattice parameters of the three alloys were determined from the {111} peaks. The lattice parameter of the powder and bar stock was determined to be $a_0 = 0.3603$ nm where the EB-DVD alloy was slightly smaller ($a_0 = 0.3557$ nm). Both are greater than the lattice parameter for pure Ni ($a_0 = 0.3524$ nm).[43] These values are close to a previously determined lattice parameter of 0.3600 nm for CPS Inconel alloy 625.[31,32] The slight lattice contraction of the vapor deposited alloy is indicative of a slightly reduced alloy element concentration. The EB-DVD alloy exhibited a decrease in the relative amount of {200} and an increase in the relative amounts of {220} oriented grains in addition to significant lattice distortion. During sintering treatments, the texture was reduced due to recrystallization of the microstructure.

D. Mechanical behavior

1. Uniaxial compression

Compressive stress–strain curves for the pressureless and the transient liquid phase sintered foams exhibited characteristics typical of metal foams, including yielding (i.e., plastic collapse) followed by a plateau region and then densification. The stress–strain curves exhibited serrated striations in the plateau region and were a result of localized fracture of individual or small groups of cells.

The normalized Young's modulus (defined as the modulus of the foam, E^*, divided by the modulus of the parent solid, E_S) and the normalized compressive yield strength (defined as the yield strength of the foam, σ^*, divided by the yield strength of the parent solid, σ_s) were measured from the stress–stain curves of samples with a range of densities, Figures 7 and 8, respectively. Also shown are Gibson and Ashby[4] theoretical relationships for the normalized Young's modulus of an open-cell reticulated foam:

$$\frac{E^*}{E_s} = k\left(\frac{\rho^*}{\rho_s}\right)^2 \quad , \tag{1}$$

where ρ^* is the density of the foam, ρ_s is the density of the parent solid, and the factor $k \approx 1.0$ for the upper bound and $k \approx 0.1$ for the lower bound.[4] A similar relationship has been developed for the normalized yield strength:

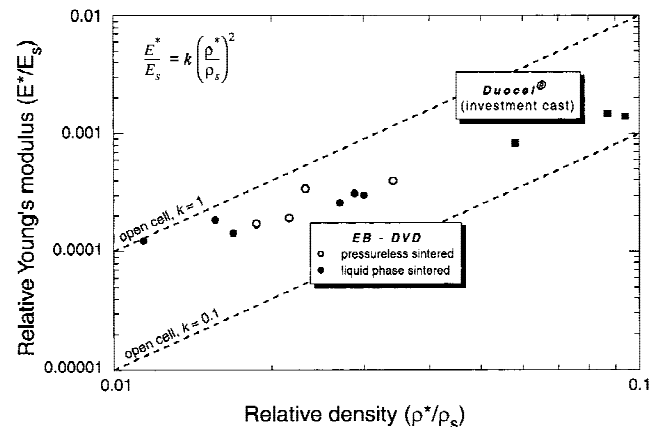$$\frac{\sigma^*}{\sigma_s} = 0.3\left(\frac{\rho^*}{\rho_s}\right)^{3/2} \quad . \tag{2}$$

FIG. 7. Normalized Young's modulus (E^*/E_S) versus relative density (ρ^*/ρ_S) for the EB-DVD Inconel alloy 625 metal foams.
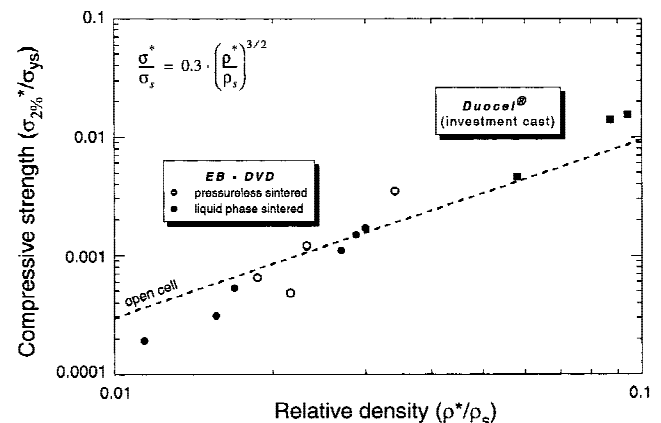

FIG. 8. Normalized yield strength (σ^*/σ_S) versus relative density (ρ^*/ρ_S) for the EB-DVD Inconel alloy 625 metal foams.

It is clear from Fig. 7 that the experimentally measured Young's moduli lie just below those predicted by Eq. (1). They fall on about the same line as investment cast foams with similar morphologies. One of the hypotheses proposed for the decreased structural performance in the elastic moduli of metal foams is the presence of imperfections such as cell wall wiggles and uneven material distribution within the cell walls, ligaments, and plateau borders.[44–46] The normalized yield strengths, shown in Fig. 8, were predicted quite well by Eq. (2).

IV. SUMMARY

An electron beam-directed vapor deposition (EB-DVD) process has been used to evaporate and deposit an Inconel alloy 625 through an open-cell, reticulated polyurethane foam for the synthesis of ultralightweight metal foams. This technique uses a combination of an electron beam gun (capable of operating in a low-vacuum environment) to generate a vapor plume and a transonic rarefied gas jet to propagate the vapor through an open-cell reticulated polymer foam. After deposition, the samples were subject to a thermal decomposition treatment to remove the polymer template. The resultant ultralightweight metal foam consisted of a fragile, three-dimensional open-cell, reticulated structure possessing hollow triangular ligaments.

The as-deposited foams were subjected to either pressureless or transient liquids phase sintering to increase their mechanical integrity. The compressive stress–strain curves for pressureless sintered and transient liquid phase sintered EB-DVD metal foams exhibited characteristics typical of metal foams, including yielding (i.e., plastic collapse) followed by a plateau region and densification. The normalized Young's modulus and yield strengths for the metal foams were predicted quite well by the Gibson and Ashby models for an open-cell reticulated foam.

ACKNOWLEDGMENTS

REFERENCES

1. M.F. Ashby, A.G. Evans, N.A. Fleck, L.J. Gibson, J.W. Hutchinson, and H.N.G. Wadley, *Metal Foams: A Design Guide* (Butterworth Heinemann, Oxford, U.K., 2000).
2. M.F. Ashby, Metall. Trans. A, **14,** 1755 (1983).
3. L.J. Gibson, Mater. Sci. Eng. A **110,** 1 (1989).
4. L.J. Gibson and M.F. Ashby, Cellular Solids: Structure and Properties, 2nd ed. (Cambridge University Press, Cambridge, U.K., 1997).
5. A.G. Evans, J.W. Hutchinson, and M.F. Ashby, Prog. Mater. Sci. **43,** 171 (1998).
6. A.G. Evans, J.W. Hutchinson, and M.F. Ashby, Curr. Opin. Solid State Mater. Sci. **3,** 288 (1998).
7. T.J. Lu and C. Chen, Acta Mater. **47,** 1469 (1999).
8. X. Wang and T.J. Lu, J. Acoust. Soc. Am. **106,** 756 (1999).
9. T.J. Lu, A. Hess, and M.F. Ashby, J. Appl. Phys. **85,** 7528 (1999).
10. T.J. Lu, H.A. Stone, and M.F. Ashby, Acta Mater **46,** 3619 (1998).
11. T.J. Lu, Int. J. Heat Mass Transfer **42,** 2031 (1999).
12. D.D. Walz, Method of Making an Inorganic Reticulated Foam Structure, U.S. Patent 3 616 841 (2 November 1971).
13. J.R. Brannan, A.S. Bean, A.J. Vaccaro, and J.J. Stewart, Continuous Electroplating of Conductive Foams, U.S. Patent 4 978 431 (18 December 1990).
14. J.R. Brannan, A.S. Bean, A.J. Vaccaro, and J.J. Stewart, Continuous Electroplating of Conductive Foams, U.S. Patent 5 098 544 (24 March 1992).
15. J.R. Brannan, A.J. Vaccaro, and J.P. Healy, High Density, High Capacity Battery Electrode, U.S. Patent 5 374 491 (20 December 1994).
16. W.A. Pruyn, Metal Foam, U.S. Patent 5 503 941 (2 April 1996).
17. W.A. Pruyn, Method for the Production of a Metal Foam, U.S. Patent 5 584 983 (17 December 1996).
18. A.J. Vaccaro, J.S. Gregg, D.W. Gibbons, J.R. Brannan, G.R. Pohto, and J.M. Hinden, Continuously Electroplated Foam of Improved Weight Distribution, U.S. Patent 5 804 053 (8 September 1998).
19. R.A. Clyde, Method of Plating Metal Uniformly on and Throughout Porous Structures, U.S. Patent 3 900 646 (19 August 1975).
20. J. Babjak, V.A. Ettel, and V. Paserin, Method of Forming Nickel Foam, U.S. Patent 4 957 543 (18 September 1990).
21. R.B. Kaplan, H.O. Pierson, R.H. Tuffias, and B.E. Williams, High Temperature Resistant Reticulated Foam Structures and Process, U.S. Patent 5 154 970 (13 October 1992).
22. G. Perugini and E. Marcaccioli, Process for the Preparation of Metallic and/or Metal-Ceramic and/or Ceramic Sponges, U.S. Patent 4 076 888 (28 February 1978).
23. E. Pinkhasov, Method of Making Open Pore Structures, U.S. Patent 4 975 230 (4 December 1990).
24. E. Pinkhasov, Method of Making Open Pore Structures, U.S. Patent 5 011 638 (30 April 1991).
25. S. Schiller, U. Heisig, and S. Panzer, Electron Beam Technology (Verlag Technik, GmbH, Berlin, Germany, 1995).
26. J.F. Groves and H.N.G. Wadley, Composites B **28,** 57 (1997).
27. D.D. Hass, H.N.G. Wadley, and Parrish, P.A., J. Vac. Sci. Technol. B **13,** 183 (1998).
28. J.F. Groves, Ph.D. Dissertation, University of Virginia (1998).
29. H.N.G. Wadley and J.F. Groves, Directed Vapor Deposition of Electron Beam Evaporant, U.S. Patent 5 534 314 (9 July 1996).
30. INCO Alloys International Inc., Product Data Sheet (1994).
31. H.K. Kohl and K. Peng, J. Nucl. Mater. **101,** 243 (1981).
32. G.K. Dey, S. Albert, D. Srivastava, M. Sundararaman, and P. Mukhopadhyay, Mater. Sci. Eng. A, **119,** 175 (1989).
33. K.K. Cushnie and S.T. Campbell, Process for Removal of Polymer Foams from Nickel-Coated Substrates, U.S. Patent 5 735 977 (7 April 1998).
34. B.A Movchan and A.V. Demchishin, Phys. Met. Metallogr. **28,** 83 (1969).

35. J.V. Sanders, in *Chemisorption and Reacting on Metal Film,* edited by J.R. Anderson (Academic Press, New York, 1971).
36. J.A. Thornton, J. Vac. Sci. Technol. **11,** 666 (1974).
37. K.A. Thornton, Annu. Rev. Mater. Sci. **7,** 239 (1977).
38. Y.G. Yang, R.A. Johnson, and H.N.G. Wadley, Acta Mater. **45,** 1455 (1997).
39. J.M. Howe, *Interfaces in Materials: atomic structure, thermodynamics and kinetic of solid-vapor, solid-liquid and solid-solid interfaces* (John Wiley & Sons, Inc., New York, 1997).
40. J.W. Cahn and J.E. Hilliard, J. Chem. Phy. **28,** 258 (1958).
41. R.M. German, *Powder Metallurgy Science* (Metal Powder Industries Federation, Princeton, NJ, 1984).
42. R.M. German, Liquid Phase Sintering (Plenum Press, New York, 1985).
43. Powder Diffraction File, Card No. 4-850, International Center for Diffraction Data (1993).
44. A.E. Simone and L.J. Gibson, Acta Mater. **46,** 3929 (1998).
45. J.L. Grenestedt, J. Mech. Phys. Solids **46,** 29 (1998).
46. R. Gradinger and F.G. Rammerstorfer, Acta Mater. **47,** 143 (1999).